Effect of a Cluster on Gas-Solid Drag from Lattice Boltzmann Simulations

Milinkumar T. Shah[1-], Ranjeet P. Utikar[1*], Moses O. Tade[1], Geoffrey M. Evans[2] and Vishnu K. Pareek[1]

[1] Department of Chemical Engineering, Curtin University, Perth, WA 6102, AUSTRALIA
[2] Department of Chemical Engineering, University of Newcastle, NSW 2308, AUSTRALIA
[*]Corresponding author's E-mail address: r.utikar@curtin.edu.au;
Telephone: +61 (8) 9266 7610; Fax: +61 (8) 9266 2681

ABSTRACT

Fast fluidization of fine particles leads to formation of particle clusters, which significantly affects the drag force between the phases. Existing gas-solid drag models, both empirical and theoretical, do not account for the effect of the clusters on the drag force, and as a result, the computational studies using them are unable to capture the inherent heterogeneity of fast fluidization beds. The limitation of the current drag models is generally attributed to poor understanding of the effect of the clusters. In this study, the effect of a single cluster on the drag force has been investigated by conducting lattice Boltzmann simulations of gas-particle flow under a wide range of the overall voidage and particle Reynolds numbers. It was observed that simulations with the particles in a cluster configuration gave considerably lower drag than those with particles in a random arrangement. Furthermore, for the cluster voidage between maximum to 0.7, a significant drag reduction was observed when the inter-particle distances within a cluster was decreased. The simulations with a constant cluster voidage of 0.7 showed that the drag force decreased on decreasing the overall voidage from the maximum voidage to approximately 0.96; however any further decrease in the overall voidage caused a steep increase in the drag force. The results of this study are important in quantifying the drag reduction due to the formation of clusters.

KEYWORDS:

Multiphase flow, Fluidization, Gas-solid drag, Mathematical modelling, Lattice Boltzmann method, Simulations

INTRODUCTION

Gas-solid flow under fast fluidization conditions underpins some important chemical processes such as fluid catalytic cracking and circulating fluidized bed combustion. Computational fluid dynamics (CFD) based gas-solid flow models have been extensively applied to investigate the hydrodynamics of fast fluidized beds and carry out possible design improvements (Sundaresan, 2000 and Ranade, 2001). All CFD models must include mass and momentum conservations for both gas and solid phases along with a model for inter-phase drag, which strongly affects the simulation results. Most commonly used empirical gas-solid drag models reasonably predict the drag force for voidage at two extremes i.e. maximum and minimum fluidizing voidage. However none of these models account for the effect of formation of particle aggregates, the so called clusters, which occurs at intermediate voidage. This work focuses on quantifying the effect of clusters on the gas-solid drag. Conventional drag models are either derived from pressure drop data under packed bed conditions e.g. the Ergun model (Ergun 1952), or from single particle settling experiments e.g. the Wen-Yu model (Wen and Yu, 1966), or a combination of these e.g. the Gidaspow drag model (Gidaspow, 1994). To account for the effect of clusters, the conventional drag models have been modified using multi-scale approaches such as sub-grid scale (Andrews IV et al., 2005) and energy minimization approaches (Li and Kwauk, 1994). Despite such modifications, the CFD models shows little qualitative agreement with experimental data (Benyahia, 2009; Shah et al., 2011). Accurate prediction of dilute gas-solid flows therefore needs improved drag models, which require better understanding of the effect of clusters. In this study, the effect of a single cluster on gas-solid drag is computationally investigated.

Available multiphase experimental techniques such as the magnetic resonance imaging, computer tomography and radioactive particle tracking are ineffective in capturing data at the spatio-temporal scales required to analyse the gas-solid interactions at cluster level. On the other hand, direct numerical simulations (DNS) of gas-particle flow can provide this information at a much smaller time and length scales (Yang et al., 2000; Hill et al., 2001; Biggs et al., 2003; Van der Hoef et al., 2005 Beetstra et al., 2007; Yin and Sundaresan, 2009; Garg et al., 2011; and Tenneti et al., 2011). Two different numerical approaches, namely lattice Boltzmann method (LBM) and immersed boundary

method (IBM) have been previously used to simulate gas-solid flow in order to study the interactions between two phases. Ladd (1994a, b) developed an effective LB method for simulating particle-fluid suspension and also LB code "SUSP3D", which has been used Hill et al. (2001a,b); Van der Hoef et al. (2005); and Yin and Sunderesan (2009). In the LBM, the flow domain is represented by a number of lattices and the fluid flow is calculated by updating velocity distribution at each lattice by using Boltzmann's velocity distribution function. The flow of particles is resolved by applying Newton's force balance equation. The force interactions between the fluid and particle are then calculated from the velocity distributions at the boundary nodes and velocity of particles. The IBM has been used by Uhlmann (2005); Garg et al. (2009) and Tenneti et al. (2011) to study the drag between the gas and solid phases. In the IBM, the fluid is represented in an Eulerian framework, whereas the particles are represented in a Lagrangian framework. The Eulerian variables are defined on a Cartesian mesh, and the Lagrangian variables are defined on a curvilinear mesh that moves freely through the cartesian mesh without being constrained to adapt to it in any way at all. The fluid-solid interactions are accounted via a smoothed approximation to the Dirac delta function (Peskin, 2002).

Hill et al. (2001a, b) used the LBM to study the drag force on spheres, and provided first numerical observations which showed that the gas-solid drag over a range of solid volume fractions was different from that calculated using the conventional drag models. However, their simulations were limited only to low particle Reynolds numbers and mono-dispersed randomly or regularly arranged particles. Van der Hoef et al. (2005) conducted LB simulations of fluid flowing past mono- and bi-disperse random arrays of spheres to measure the drag force on the spheres for a range of volume fractions and particle Reynolds number. They proposed a correlation for the drag force applicable to both mono- and poly-disperse systems. Beetstra et al. (2006) further extended the LBM study by simulating particles arranged in cluster configurations. The numerically calculated drag coefficients were compared with the experimental data of drag coefficients for irregularly shaped particles reported by Tran-Cong et al. (2004). Beetstra et al. (2006) predicted a strong effect of inter-particle distance on the gas-solid drag force. However, this study was limited only up to 32 particles, and did not include the effect of particle Reynolds number on the drag force. Most of the simulations carried

out by Beetstra et al. (Van der Hoef et al., 2005; and Beetstra et al., 2006) used a constant particle resolution in all simulations, including those with higher Reynolds number. At higher Reynolds numbers their resolution was not sufficient to resolve the boundary layer thickness around the particle resulting into erroneous drag values. This has been critically highlighted by Tenneti et al. (2011). Tenneti et al. (2011) also strongly suggested requirement of high resolution LBM simulations. Yin and Sunderesan (2009) used the LBM to simulate flow with mono- and bi-dispersed particles, and gave a drag correlation for Stokes flow in fixed particle configuration. Recently, Zhang et al. (2011) simulated a 2D periodic array of clusters using the LBM to investigate the effect of cluster on the drag coefficient. They found close agreement between the simulated drag values and those calculated from the energy minimization approach.

While there are several detailed gas-solid flow simulations, the effect of clusters on the gas-solid drag is still poorly understood. The present study aims to quantify the effect of a single cluster on gas-solid drag by conducting high resolution 3D LB simulations. The simulated flow domain was a cube with periodic boundary conditions, where solid particles were positioned in either random or a cluster configurations. In the cluster configuration, most of particles (up to 1000) were positioned close to each other forming a single cluster with few particles located around the cluster forming a dilute phase. Simulations were carried out with different cluster configurations by varying both overall voidage of the flow domain and voidage of cluster. Furthermore, the flow conditions in these simulations were also varied to cover a wide range of particle Reynolds number from 21 to 210. Simulations results were the drag forces for both the flow domain with random and cluster configurations, which were compared and analysed in order to quantify the effect of a cluster.

LATTICE BOLTZMANN METHOD

This section is intended to give a brief introduction to the LBM for modelling of multiphase flows. For a more detail understanding of the LBM for multiphase flows, readers are referred to Ladd (1994a and b) and Van der Hoef et al. (2005). LBM is a direct numerical simulation technique which resolves the flow of fluid by solving the Boltzmann equation of velocity distributions. The movement of particles is calculated by solving Newton's force balance equation for each particle. The

momentum exchange between the fluid and particles is resolved by applying the bounce back rules at boundary nodes.

Flow of fluid: Flow domain is as number of discrete lattice nodes in x, y and z directions. Each node represents a fluid element with its velocity distributed in 19 directions (D3Q19). At each fluid element, the velocity distribution is updated by the Boltzmann equation:

$$f_a(x + e_a, t + \Delta t) = f_a(x, t) - \frac{[f_a(x,t) - f_a^{eq}(x,t)]}{\tau/\Delta t} \quad \text{eq. (1)}$$

where f_a is velocity distribution at any lattice node x, e_a is the direction vectors, τ is a relaxation time, and Δt is the time for the fluid elements to travel from node to node. The velocity distribution function, $f_a(x,t)$, describes number of gas elements at lattice node x and time t with a velocity in e_a direction. The magnitudes of velocity direction vectors e_0, $e_{1\text{-}6}$ and $e_{7\text{-}19}$ are 0 (particle at rest), 1 and $\sqrt{2}$ respectively.

Equation (1) has two parts, where (i) $f_a(x + e_a, t + \Delta t) = f_a(x, t + \Delta t)$ represents streaming; and (ii) $f_a(x, t + \Delta t) = f_a(x, t) - [f_a(x,t) - f_a^{eq}(x,t)]/(\tau/\Delta t)$ represents collision steps. Collision is represented by a relaxation towards equilibrium, and the relaxation time controls the kinematic viscosity of the LB fluid (Bhatnagar et al., 1954).

The most common approach to model the relaxation is the Bhatnagar-Gross-Krook (BGK) approach (Bhatnager et al., 1954); where the relaxation time, τ is governed by the kinematic viscosity of the fluid, with length being represented in terms of lattice units or the distance between two neighbouring lattice nodes, i.e.;

$$\tau = 3v + 0.5 \quad \text{eq. (2)}$$

where v is the kinematic viscosity of fluid in lu^2/ts.

Another method for modelling the relaxation is to use the stress tensor update (Ladd, 1994a, b):

$$\Pi'_{\alpha\beta} = \Pi^{eq}_{\alpha\beta} + (1+\lambda)\left(\bar{\Pi}_{\alpha\beta} - \bar{\Pi}^{eq}_{\alpha\beta}\right) + \frac{1}{3}(1+\lambda_B)(\Pi_{\gamma\gamma} - \Pi^{eq}_{\gamma\gamma})\delta_{\alpha\beta} \quad \text{eq. (3)}$$

where Π' is the stress tensor after collision, and Π is the stress tensor before collision. Furthermore, λ and λ_B are related to the shear viscosity and bulk viscosity respectively. Their relation with the relaxation time can be given by:

$$\lambda = 1 - \frac{1}{\tau} \quad \text{eq. (4a)}$$

$$\lambda_B = 1 - \frac{1}{\tau_\Sigma} \quad \text{eq. (4a)}$$

In our simulations, the values of λ and λ_B are set to -0.99 and -1 respectively, which corresponds to the value of the kinematic viscosity equal to 0.0008333 (Ladd and Verberg, 2001; Van der Hoef et al., 2005). Macroscopic properties such as density, velocity and stress are calculated from the velocity distribution functions at each lattice node using the following equations,

$$\rho = \sum_{\alpha=0}^{19} f_\alpha \quad \text{eq. (5a)}$$

$$u = \sum_{\alpha=0}^{19} f_\alpha e_\alpha \quad \text{eq. (5b)}$$

$$\pi = \sum_{\alpha=0}^{19} f_\alpha e_\alpha e_\alpha \quad \text{eq. (5c)}$$

The macroscopic properties are used to calculate equilibrium distribution:

$$f_\alpha^{eq} = w^{e_\alpha}\rho\left[1 + \frac{ue_\alpha}{c_s^2} + \frac{(ue_\alpha)^2}{2c_s^4} - \frac{u^2}{2c_s^2}\right] \quad \text{eq. (6)}$$

where c_s is the speed of sound and w^{ea} is the weight function for different directions. The value of c^2_s is 1/3 lattice unit per second, whilst those of w^0, w^1 and $w^{\sqrt{2}}$ are 1/3, 1/18 and 1/36 respectively (Ladd and Verberg, 2001; and Van der Hoef et al., 2005).

Fluid-solid interactions:

The solid boundary can be located either at the lattice node or nodes middle of the links between lattice nodes. In the present study spherical particles are mapped on the discrete lattices using boundary nodes which are located only at the middle of the links between lattice nodes. Similarly, stationary solid boundaries are selected to be in the middle of two lattice points (Ladd and Verberg, 2001; and Van der Hoef et al., 2005).

When a fluid element encounters a stationary solid boundary, bounce back rule is applied, i.e.:

$$f_{-\alpha}(x, t + \Delta t) = f_{\alpha}(x, t) \qquad \text{eq. (7)}$$

This results in a fluid velocity of zero in the middle of two boundary sites, corresponding to no-slip velocity conditions at stationary walls.

If a fluid element strikes a moving solid boundary, such as suspended particles, then the bounce back rule is modified to accommodate the velocity at the boundary node. The bounce back rule at the moving solid boundary can be given as:

$$f_{-\alpha}(x, t + \Delta t) = f_{\alpha}(x, t) - 6\rho_w w^{e\alpha}(u_b e_{\alpha}) \qquad \text{eq. (8)}$$

where ρ_- is wall density, and u_b is the velocity of the boundary nodes inside the particle. The value of u_b is resultant of the axial and radial velocity of the particle, given by:

$$u_b = U + \Omega \times (r_b - R) \qquad \text{eq. (9)}$$

where U is translation velocity of the particle, Ω is angular velocity, r_b is location of boundary node and R is the location of centre of mass of the particle.

The resulting force exerted by the fluid element on the particle because of the change in momentum of the fluid element is given by:

$$F_{f-p} = \sum_b \sum_{\alpha} [2 f_{\alpha}(x, t) - 6\rho_w w_{\alpha}(u_b e_{\alpha})] e_{\alpha}; \qquad \text{eq. (10)}$$

whilst torque is given by:

$$T_{f-p} = \sum_b (r_b - R) \sum_a [2f_a(x,t) - 6\rho_w w_a (u_b e_a)] e_a \quad \text{eq. (11)}$$

where Σ_a and Σ_b represent summation over all nineteen directions and boundary nodes respectively.

Movement of particles: Newton's force balance equation is solved for each particle to obtain its velocity:

$$F_p = M_p \frac{d}{dt} U \quad \text{eq. (12)}$$

$$T_p = I_p \frac{d}{dt} \Omega \quad \text{eq. (13)}$$

where F_P and T_P are momentum and torque transfers to particles from fluid plus other forces. M_p and I_p are mass and moment of inertial of the particle.

The change in fluid momentum (eq. 8) at the boundary nodes on a single particle is equal and opposite of the total force that the gas exerts, $F_{f\text{-}s}$. Using this equality, the drag force F_d can be calculated.

The force exerted by the gas on each particle (eq.10) is multiplied by overall voidage to calculate the drag force on each particle (Van der Hoef et al., 2005).

$$F_d = \varepsilon F_{f-p} \quad \text{eq. (14)}$$

The drag force is then normalized by the Stokes-Einstein drag ($\mathrm{Fd} = 3\pi\mu dU$) to define the dimensionless drag force.

$$F_{d,normalized} = \frac{F_d}{3\pi\mu dU} \quad \text{eq. (15)}$$

LB SIMULATIONS

For the present work, a multiphase 3D lattice Botzmann code "SUSP3D" (Ladd, 1994a and b) is used. SUSP3D is a highly parallel code and scales well for thousands of particles. However, the size of the flow domain and number of particles in simulations are limited by the available computational power. For example, to simulate 1000 particles at 0.7 voidage and 105 $N_{Re,p}$ with resolution of 42 lattices per particle requires a flow domain of 630 lattices in each direction and 12000 CPU hours on intel Xeon 2.93GHz CPU The simulations were carried out over a periodic domain for 250 to 500 cycles. For each cycle, the normalized drag force was averaged over all particles. The averaged normalized drag force for last 100 cycles was to calculate the ensemble-averaged normalized drag.

$$F_{d,normalized,avg} = \sum_{i=1}^{n} F_{d,normalized} \qquad \text{eq. (16)}$$

$$F_{d,normalized,ensamble-avg} = \sum_{i=1}^{c} F_{d,normalized,avg} \qquad \text{eq. (17)}$$

where $F_{f\text{-}p}$ is total force on each particle, F_d is drag force on a single particle, $F_{d,normalized}$ is the dimentionless normalized drag force, μ is viscosity of fluid, d is diameter of particle and U is superficial velocity of fluid.

Simulations with both random and cluster configurations were performed. In random configuration, the particles were randomly positioned using the Monte-Carlo method in a cubical flow domain (Figure-1a); whereas cluster configurations have particle positioned close to each other forming a single cluster with few particles located around the cluster forming a dilute phase (Figure-1b),

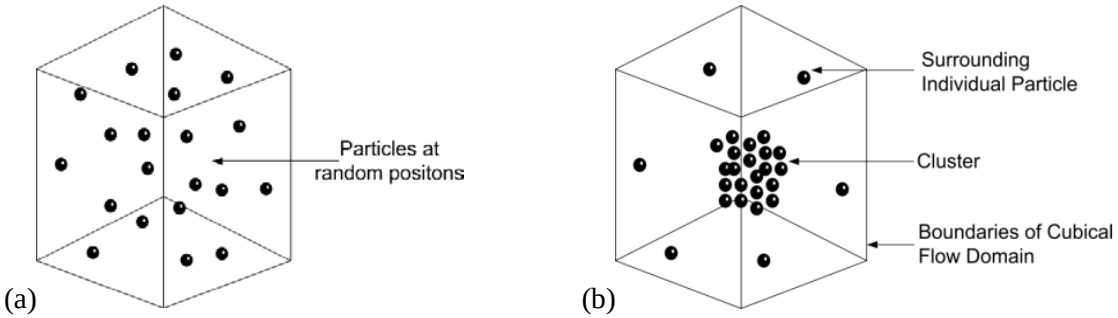

Figure 1: Particles in (a) random configuration (b) cluster configuration

206 The simulations were initially verified by comparing the calculated drag force from the simulations of
207 this study to that reported by two previous numerical studies i.e. (i) Beetstra (2006) and (ii) Tenneti et
208 al. (2011).Three different random configurations were prepared using the Monte-Carlo method from
209 three initial configurations with i.e. (i) 32 particles in face centric cubical (FCC); (ii) 54 particles in
210 body central cubical (BCC); and (iii) 64 particles in simple cubical (SC) structure and then displacing
211 the particles from their initial positions. A single particle was resolved using 16.4 lattices for
212 comparison with Beetstra et al. (2005) and 20-58 lattices for comparison with Tenneti et al. (2011).
213 The size of the flow domain was adjusted to achieve a desired volume fraction.

Table 1: Simulation conditions

	Initial simulations		Simulations with cluster configurations
	Comparison with Beetstra, 2005	Comparison with Tenneti et al., 2011	
Flow domain	Variable	Variable	Variable
Particle diameter	16.4 lu	20 – 58 lu	20 – 58 lu
Kinematic viscosity	8.333e-4 lu	8.333e-4 lu	8.333e-4 lu (Ladd, 1991a, b)
Fluid density	36 lu	36 lu	36 lu (Van der Hoef et al., 2005)
Particle arrangement	Random	Random	Cluster Configuration
Number of particle	32-64	32-64	90-1000
Particle Reynolds Number	0.2 and 21	21-210	21-210

214 After verification, simulations were carried out for cluster configurations (shown in Figure-1 and
215 Table-2). The volume of cluster was calculated from the number of particles in a cluster, volume of
216 each particle and cluster voidage (eq. 19). Similarly, the volume of flow domain was calculated using
217 total number of particles (that in both cluster and surrounding) and overall voidge (eq. 20).
218 Surrounding particles were randomly positioned in a space between boundaries of the cluster and flow
219 domain.

$$V_c = \frac{N_c V_p}{(1-\varepsilon_c)} \quad \text{eq. (18)}$$

$$V = \frac{N V_p}{(1-\varepsilon)} \quad \text{eq. (19)}$$

where V_c is the volume of cluster, N_c is the number of particles in a cluster, V_p is the volume of each particle, V is the volume of flow domain, N is the number of particles in a cluster, ε is overall voidage, and ε_c is cluster voidage.

Table 2: Details of Particle Configurations

	particles	particles in cluster	particles in surrounding	Cluster voidage	Overall voidage	Cluster fraction
1	90	64	26	0.9	0.985-	0.15
2	90	64	26	0.8	0.985-	0.075
3	90	64	26	0.7	0.985-	0.05
4	90	64	26	0.6	0.985-	0.0375
5	90	64	26	0.5	0.985-	0.03
6	151	125	26	0.7	0.98	0.0667
7	242	216	26	0.7	0.96	0.1333
8	538	512	26	0.7	0.91	0.3
9	1000	1000	26	0.7	0.85	0.5

Voidage reported in Table 3 are calculated using Equation 14 (Li and Kwauk, 1994):

$$\varepsilon = (1-f)\varepsilon_f + f\varepsilon_c \quad \text{eq. (20)}$$

where ε is overall voidage, f is cluster fraction, ε_f is voidage of surrounding fluid and ε_c is cluster voidage. Note that due to small number of particles present, the voidage of surrounding fluid, ε_f, is generally assumed to be close to unity.

$$f = \frac{1-\varepsilon}{1-\varepsilon_c} = \frac{V_c}{V} \quad \text{eq. (21)}$$

The particle configuration was initialized to move with a certain velocity (v_{sim}) in an arbitrary direction. As a result, the moving particles exerted force on the gas phase, which was counterbalanced by applying uniform back force to the gas phase by setting backflow velocity (u) for the gas phase (Van der Hoef et al., 2005).

$$(1-\varepsilon)V\rho_s v_{sim} + \varepsilon V \rho u = 0 \quad \text{eq. (22)}$$

where v_{sim} is the velocity of the particle configuration, u is backflow velocity of the gas phase, ρ is a density of the gas phase and ρ_s is density of the solid. The ratio of densities of the gas and solid phases was set to 1 (Van der Hoef et al., 2005), and as a result:

$$\varepsilon(u - v_{sim}) = -v_{sim} = U \quad \text{eq. (23)}$$

where U is the superficial velocity of the gas. The particle Reynolds number of the gas-solid flow was then calculated by,

$$N_{Re,p} = \rho U d/\mu = \rho V_{sim} d/\mu. \quad \text{eq. (24)}$$

For a specific particle configuration and particle Reynolds number, seven independent simulations were conducted with velocities in seven different directions, namely, x, y, z, xy, xz, yz and xyz. The calculated normalized drag force from these seven simulations was averaged and reported with error bars showing the variation in the values.

RESULTS

To verify the simulation methodology, results from random particle arrangement were compared with those reported by Beetstra (2005). Figure-2(a) and (b) shows a comparison between the calculated drag forces from our simulations and those reported by Beetstra (2005) for low (0.2) and high (21) particle Reynolds numbers respectively. The simulation results closely agree with those from Beestra (2005). Figure-2 also shows comparison between the calculated normalized drag and empirical drag

253 models such as the Ergun and Wen-Yu models (Wen and Yu, 1966). At very high overall voidage
254 (close to unity), the calculated drag forces from both this study and Beetstra (2005) reasonably agreed
255 with that calculated from the Wen-Yu model. At low voidage close to minimum fluidizing voidage
256 simulations from this study and Beetstra (2005) show discrepancies with the Ergun model (Ergun,
257 1952). It was also observed that the drag from the LB simulations were considerable different from
258 that from the empirical drag models, particularly at lower voidage. Such differences between
259 numerically and empirically calculated drag values were also observed by Hill et al. (2001) and
260 Beetstra (2005).

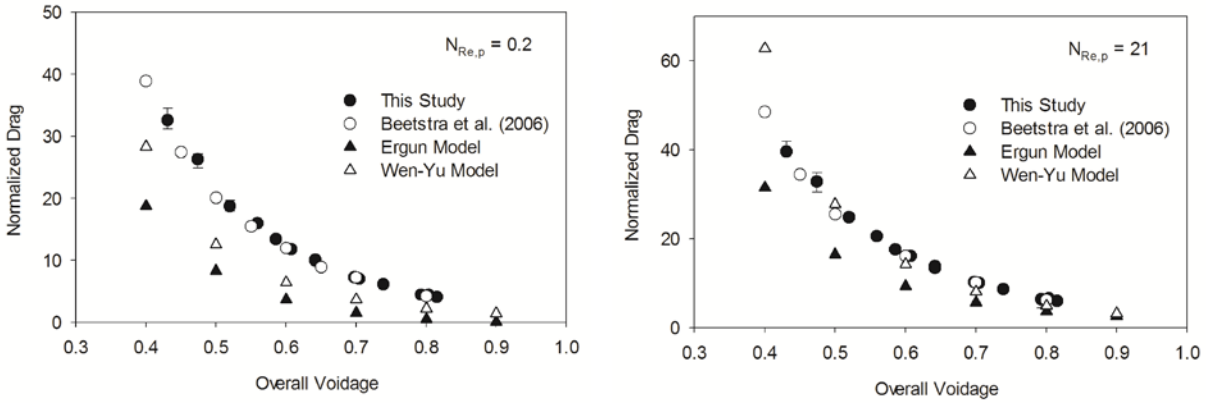

(a) (b)

Figure 2: Normalized drag force Vs. Overall voidage

261 Beetstra (2005) used a low particle resolution of 16.4 to 24.4 lattices for both low and high Reynolds
262 number simulations. This particle resolution is adequate at lower particle Reynolds numbers, but it
263 does not resolve the boundary layer around particle at higher particle Reynolds numbers. Particle
264 resolution is particularly critical at high volume fractions when the gap between two particles is
265 narrow and at high Reynolds numbers where the boundary layer thickness is very thin (Tenneti et al.,
266 2011). Van der Hoef (2005) noted that an asymptotic value of the normalized drag force could be
267 obtained from LBM simulations by performing consecutive simulations at higher grid resolutions and
268 then extrapolating the results to $1/r_h^2 \rightarrow \infty$, where r_h represents the gap between the two particles. As
269 the particle resolution increases, computational demands of the LBM increase exponentially. Thus
270 performing successive simulations soon becomes impractical, especially for high particle Reynolds
271 numbers where particles need to be resolved using a large number of lattices.

Tenneti et al. (2011) conducted immersed boundary simulations of gas-particle suspension and found discrepancies between their results and those reported by Beetstra (2005). They attributed these discrepancies to inability of Beetstra's (2005) simulations to resolve the boundary layer.

Table 3: Grid resolutions used in this study

$N_{Re,p}$	D (lu)	$\delta = D/\sqrt{N_{Re,p}}$ (lu)	ε	D (lu)	$r_h = D\varepsilon/6(1-\varepsilon)$ (lu)
21	20	~4	0.5	20	~3
42	26	~4	0.5	26	~4
84	37	~4	0.5	37	~6
105	42	~4	0.5	42	~7
210	58	~4	0.5	58	~9

In our simulations, the grid resolution was varied with the particle Reynolds number to adequately capture the gap between the two particles ($r_h = D\varepsilon/6(1-\varepsilon)$ and the boundary layer thickness ($\delta = D/\sqrt{N_{Re,p}}$) with sufficient number of lattices. The grid resolution for different conditions is shown in Table-3. Simulations with these grid resolutions were carried out and compared with the results presented by Tenneti et al. (2011). The comparison shows good agreement between the two results (Figure-3). These particle resolutions (Table-3) were then used for all consequent simulations with cluster configurations. In these simulations, each particle was represented by 20-58 lattices depending on the particle Reynolds number (Table-3); whereas the domain size was around 15 times of particle size. This approximately corresponds to the grid size in continuum gas-solid flow simulations. For example, a 60 micron particle represented by 20 lattice units, the domain size will be ~300 lattice units in each directon, where 1 *lu* corresponds to 3 microns

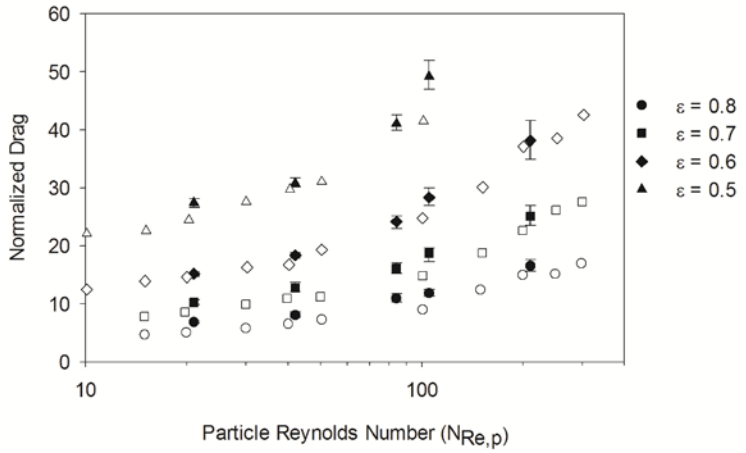

Figure 3: Normalized drag Vs. particle Reynolds number (○, □, ◊, Δ – Tenneti et al., 2011; and ●, ■, ♦, ▲ – This Study)

Effect of a cluster on gas-solid drag

After the initial verification, simulations were carried out for random and configurations. The random configuration consisted of 108 particles, whereas the cluster configurations had 90 particles with 64 particles forming a single cluster and 26 particles randomly placed in surrounding. The details of the configuration are given in Table-2 (first 5 configurations). Simulations were carried out with constant particle Reynolds number and overall voidage and corresponding cluster fraction. The resulting normalized drag force is shown in Figure-4(a). At higher cluster voidage (> 0.9), the calculated normalized drag force approached the value obtained for the random configuration. Between the cluster voidage of 0.985 and 0.7, the calculated normalized drag force steeply declined with decrease in the cluster voidage. However, further reduction in the cluster voidage from 0.7 resulted into only gradual reduction in drag force. These observations were consistent in simulation results at different particle Reynolds number. Based on these results, a fixed value of the cluster voidage of 0.7 was used in subsequent simulations for further investigations.

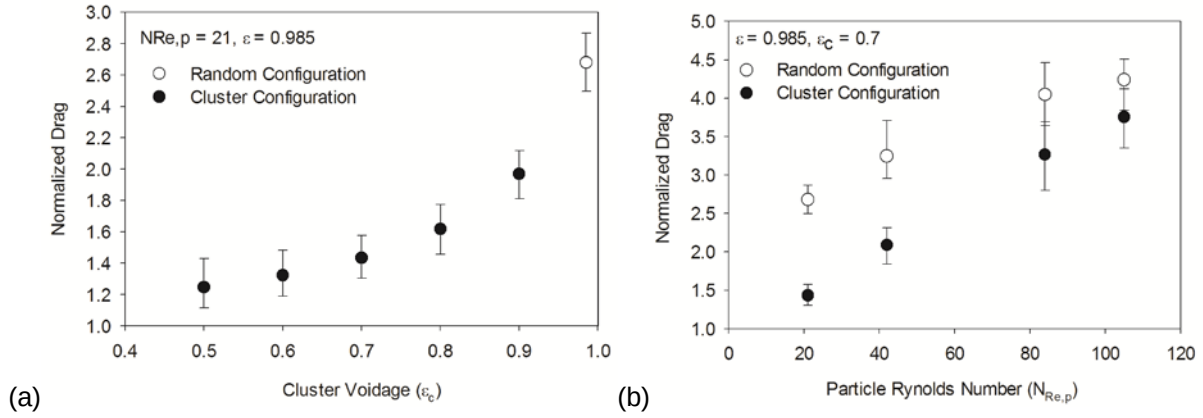

Figure 4: (a) Normalized drag Vs. Cluster voidage; (b) Normalized drag Vs. particle Reynolds number

Figure-4(b)shows a comparison between calculated drag forces from (i) random configuration of 108 particles and (ii) cluster configuration of 90 particles with a constant cluster voidage equal to 0.7 (third configuration in Table-2). The overall voidage in these simulations was constant at 0.985, whilst the particle Reynolds number varied from 21 to 105. The simulation results show that the drag for the cluster configuration was significantly lower than that for the randomly arranged particle configuration over the entire range of the particle Reynolds numbers. Moreover, the difference in drag between two configurations reduced with increase in the particle Reynolds number. The observed drag reduction with the cluster configuration was qualitatively coherent with the drag from the energy minimization multi-scale (EMMS) concept (Li and Kwauk, 1994); which says that the formation of clusters causes less resistance to the flow of the fluid, and as a result it decreases the effective drag force. The simulation results also provide a basis for quantifying such a reduction.

Effect of overall voidage and cluster fraction

Clusters in dilute gas-solid flows can consist of more than 1000 particles (Shaffer et al., 2010). Simulations were therefore conducted with increasing number of particles in a cluster, from 64 to 1000 keeping number of surrounding particles constant. Six particle configurations (see configurations 3 and 6-10, Table-2) were considered. Each configuration had a different overall voidage but the same cluster voidage of 0.7. Such an arrangement resulted in a variation in cluster

fraction from 0.05 to 0.75. Figure-5 shows the effect of overall voidage and cluster fraction on the calculated normalized drag force. It can be seen that as the overall voidage was increased, the solid phase resistance decreased which lowered the normalised drag. However, beyond the overall voidage of approximately 0.96, an increase in the normalized drag force was observed. This is due to the cluster behaviour transiting into randomly arranged particles at very high voidage, resulting in the normalized drag force approaching the value calculated for randomly arranged particles at the maximum voidage. As the overall voidage reduced below 0.96, the increase in cluster fraction showed steep increase in the drag force. At lower overall voidage, the drag force approaches the value for randomly arranged particles with approximately 0.85 overall voidage. The results suggest that calculated normalized drag force formed minimum at the overall voidage of ~0.96 with its value increased with both increase and decrease in the overall voidage from 0.96.

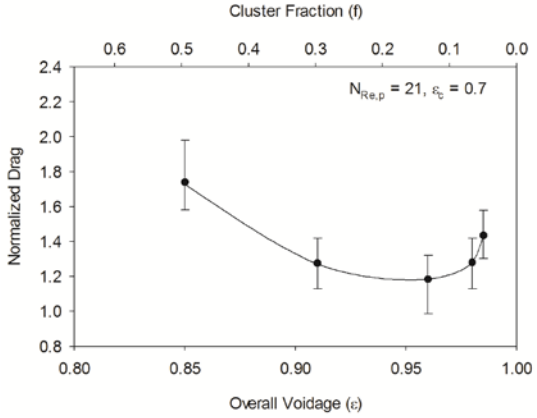

Figure 5: Normalized drag force Vs. Overall voidage

Simulations were also carried out at different particle Reynolds numbers to study the effect of the overall voidage and cluster fraction at constant cluster voidage. Figure-6 shows the calculated normalized drag calculated from simulations of six particle configurations (see configurations 3 and 6-10, Table-3) with different particle Reynolds numbers ranging from 21-105. For all simulations, a minimum drag force in the range 0.95-0.96 overall voidage was obtained with the minimum value of the drag force was found to increase with increased particle Reynolds numbers. Here, the prediction of minimum drag at particular overall voidage resembles the calculated drag using the EMMS approach (Yang et al., 2004). However in the EMMS, the position of the minimum drag in reference

to the overall voidage highly dependent on operating flow conditions, as well as the use of cluster diameter correlations (Shah et al., 2011)

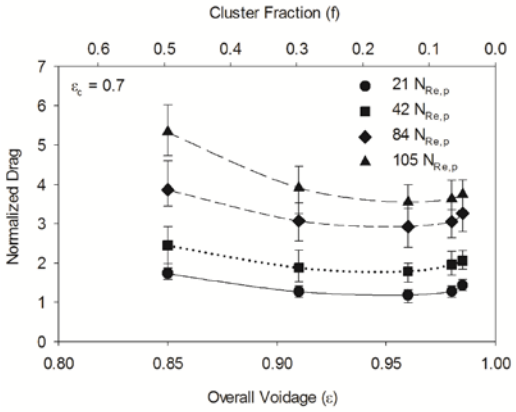

Figure 6: Normalized drag force Vs. Overall voidage

The simulations carried out as part of this study depended on (i) overall voidage, (ii) particle Reynolds number, (iii) cluster fraction, and (iv) cluster voidage. Overall voidage, cluster voidage and cluster fraction are related by eq. (20). Hence, flow can be defined by knowledge of three parameters. Information on the cluster voidage at given flow conditions is not available either experimentally or numerically. In the present study the cluster voidage was assumed to be constant. Work on predicting the cluster formation and cluster configuration for a given set of flow conditions is currently under progress.

CONCLUSION

Gas-particle flow with the particles arranged in the cluster configurations and random arrangements was simulated using the LBM to investigate the effect of a single cluster and its properties on the drag force over a wide range of voidage and particle Reynolds numbers. Simulations were validated using previously published results by Beetstra (2005) and Tenneti et al. (2011).

The simulation results showed that the calculated drag forces from the simulations with the particles arranged in the cluster configuration was considerably lower than that from the simulations with randomly arranged particles under the same flow conditions. The reduction in the calculated drag force in the flow with the cluster was observed to be larger at the lower particle Reynolds numbers. The simulations with different particle configurations with varying inter-particle distances in the

cluster and a constant overall voidage showed that a major drag reduction happened for the cluster voidage higher than 0.7, whereas a minor decrease in the drag force was observed for the cluster voidage less than 0.7. When simulations were conducted at a constant cluster voidage of 0.7, the drag decreased on decreasing the overall voidage from the maximum voidage to approximately 0.96; however any further decrease in the overall voidage resulted in a steep increase in the calculated drag force. The results of this study are important in quantifying the drag reduction caused by the formation of the cluster, and they are also useful in formulating an improved drag correlation for CFD simulations.

ACKNOWLEDGEMENT

Authors would like to acknowledge Prof. Anthony J. C. Ladd for SUSP3D code. The work was supported by iVEC through the use of advanced computing resources located at iVEC@Murdoch. This work was part of ARC funded research grant LP110100717.

NOMENCLATURE

c_s	Speed of sound (lu/s)
D	Number of lattices per particle
e_a	Direction vector
F	Momentum (kg m/s)
F_d	Drag force (kg m/s^2)
f	Cluster fraction
f_a	Velocity distribution function
$N_{Re,p}$	Particle Reynolds number
M	Mass (kg)
r_b	Location of boundary node [lattice unit(lu)]
r_h	Hydrodynamic diameter (lu)
R	Location of centre of mass of a particle (lu)
T	Torque (kg m^2/s^2)

380	t	Time (s)
381	Δt	Time step (s)
382	U	Superficial velocity (lu/s)
383	U	Velocity of particle (lu/s)
384	u	macroscopic velocity (lu/s)
385	u_b	Velocity at boundary node (lu/s)
386	x	Lattice node
387	Δx	Gap between two lattice node (lu)
388	v	Kinematic viscosity
389	w	Weight functions
390	*Greek Lettter*	
391	ε	Voidage
392	ρ	Macroscopic Density (kg/m^3)
393	τ	Relaxation time (s)
394	μ	Viscosity (kg/m s)
395	π	Macroscopic stress
396	Π	Stress tensor
397	Ω	Angular velocity
398	*Subscript*	
399	a	Direction
400	b	Boundary
401	c	Cluster
402	d	Drag
403	eq	Equilibrium
404	f	fluid
405	f-p	Exchange between fluid and particle
406	f-s	Exchange between fluid and solid
407	p	Particle

REFERENCES

Sundaresan, S., 2000. Modeling the hydrodynamics of multiphase flow reactors: current status and challenges. AIChE Journal 46, 1102-1105.

Ranade, V.V., 2001. Computational flow modeling for chemical reactor engineering. Academic Press.

Gidaspow, D., 1994. Multiphase flow and fluidization: continuum and kinetic theory descriptions. Academic Press.

Ergun, S., 1952. Fluid flow through packed columns. Chemical Engineering Progress, 48**,** 89-94.

Wen, C. Y. and Yu, Y. H., 1966. Mechanics of fluidization. Chemical Engineering Progress Symposium Series.

Andrews IV, A.T., Loezos, P.N., Sundaresan, S., 2005. Coarse-grid simulation of gas-particle flows in vertical risers. Industrial & Engineering Chemical Research **44**, 6022-6037.

Li, J., and Kawauk, M., 1994. Particle-fluid two-phase flow: The energy-minimization multi-scale method. Metallurgical Industry Press.

Benyahia, S., 2009. On the Effect of Subgrid Drag Closures. Industrial & Engineering Chemistry Research **49**, 5122-5131.

Shah, M.T., Utikar, R.P., Tade, M.O., Evans, G., Pareek, V.K., 2011. Simulation of gas-solid flows in riser using energy minimization multiscale model: Effect of cluster diameter correlation. Chemical Engineering Science, **66**, 3391-3300.

Yang, R., Zou, R., Yu, A., 2000. Computer simulation of the packing of fine particles. Physical review E 62, 3900.

Hill, R.J., Koch, D.L., Ladd, A.J.C., 2001a. The first effects of fluid inertia on flows in ordered and random arrays of spheres. Journal of Fluid Mechanics, **448**, 213-241.

Hill, R.J., Koch, D.L., Ladd, A.J.C., 2001b. Moderate-Reynolds-number flows in ordered and random arrays of spheres. Journal of Fluid Mechanics, **448**, 243-278.

Biggs, M.J., Humby, S.J., Buts, A., Tüzün, U., 2003. Explicit numerical simulation of suspension flow with deposition in porous media: influence of local flow field variation on deposition processes predicted by trajectory methods. Chemical Engineering Science, **58**, 1271-1288.

Van der Hoef, M., Beetstra, R., Kuipers, J., 2005. Lattice-Boltzmann simulations of low-Reynolds-number flow past mono-and bidisperse arrays of spheres: results for the permeability and drag force. Journal of Fluid Mech 528, 233-254.Beetstra, R., Van der Hoef, M., Kuipers, J., 2007. Drag force of intermediate Reynolds number flow past mono-and bidisperse arrays of spheres. AIChE Journal 53, 489-501.

Yin, X., Sundaresan, S., 2009. Fluid-particle drag in low-Reynolds-number polydisperse gas–solid suspensions. AIChE Journal 55, 1352-1368.

Garg, R., Tenneti, S., Yusof, J.M., Subramaniam, S., 2011. Direct numerical simulation of gas-solids flow based on the immersed boundary method. Computational Gas-Solids Flows and Reacting Systems: Theory, Methods and Practice.

Tenneti, S., Garg, R., Subramaniam, S., 2011. Drag law for monodisperse gas–solid systems using particle-resolved direct numerical simulation of flow past fixed assemblies of spheres. International Journal of Multiphase Flow 37, 1072-1092.

Uhlmann, M., 2005. An immersed boundary method with direct forcing for the simulation of particulate flows. Journal of Computational Physics 209, 448-476.

Peskin, C.S., 2002. The immersed boundary method. Acta numerica 11, 479-517.

Ladd, A. J. C., 1994. Numerical simulations of particulate suspensions via a discretized Boltzmann equation. Part 1. Numerical results. Journal of Fluid Mechanics, **271**, 285-309.

Ladd, A. J. C., 1994. Numerical simulations of particulate suspensions via a discretized Boltzmann equation. Part 2 Numerical results. Journal of Fluid Mechanics, **271**, 311-339.

Beetstra, R., Van Der Hoef, M. A., Kuipers, J. A. M., 2006. A lattice-Boltzmann simulation study of the drag coefficient of clusters of spheres. Computers & Fluids, **35**, 966-970.

458 Zhang, Y., Ge, W., Wei Wang, X., He Yang, C., 2011. Validation of EMMS-based drag model
459 using lattice Boltzmann simulations on GPUs. Particuology, **9**, 365-373.

460 Bhatnagar, P. L., Gross, E. P., Krook, M., 1954. A model for collision processes in gases. I. Small
461 amplitude processes in charged and neutral one-component systems. Physical Review, **94**, 511.

462 Ladd, A., Verberg, R., 2001. Lattice-Boltzmann simulations of particle-fluid suspensions. Journal of
463 Statistical Physics 104, 1191-1251.

464 Beetstra, R., 2005. Drag force in random arrays of mono-and bi-disperse spheres. PhD, University of
465 Twente.

466 Shaffer, F., Gopalan, B., Breault, B., Cocco, R., Hays, R., Karri, R., Knowlton, T., 2010. A New
467 View of Riser Flow Fields Using High Speed Particle Imaging Velocimetry (PIV), 2010 AIChE
468 Annual Meeting. AIChE, Salt Lake City, UT, US.